37. Y. Cang *et al.*, *Cell* **127**, 929 (2006).
38. Y. Cang *et al.*, *Proc. Natl. Acad. Sci. U.S.A.* **104**, 2733 (2007).
39. We thank T. Wada, S. Sakamoto, and S. Ishihara for discussions; P. Raychaudhuri, T. Matsunaga, S. Krauss, B. Thisse, A. Kawakami, S. Noji, J. Izpisua-Belmonte, K. Kawakami, and J. Yamauchi for valuable reagents; Y. Tsuboi for technical support; and P. Sharp and A. Berk for comments on this manuscript. This work was supported by Special Coordination Funds for Promoting Science and Technology from JST, by the Global COE (Center of Excellence) Program from the Japan Ministry of Education, Culture, Sports, Science, and Technology (MEXT), and by a grant for Research and Development Projects in Cooperation with Academic Institutions from the New Energy and Technology Development Organization (H.H. and H.A.). This work was also supported by grants-in-aid for Scientific Research (20370084 to T.O.) and for Young Scientists (21770226 to T.S.) from MEXT and by the Precursory Research for Embryonic Science and Technology program from JST (T.S.). T.I. was a Japan Society for the Promotion of Science Research Fellow. An application for a patent has been filed in the Japan Patent Office.

Supporting Online Material
www.sciencemag.org/cgi/content/full/327/5971/1345/DC1
Materials and Methods
SOM Text
Figs. S1 to S19
Tables S1 and S2
References

5 June 2009; accepted 10 February 2010
10.1126/science.1177319

REPORTS

Variations in the Sun's Meridional Flow over a Solar Cycle

David H. Hathaway[1]* and Lisa Rightmire[2]

The Sun's meridional flow is an axisymmetric flow that is generally directed from its equator toward its poles at the surface. The structure and strength of the meridional flow determine both the strength of the Sun's polar magnetic field and the intensity of sunspot cycles. We determine the meridional flow speed of magnetic features on the Sun using data from the Solar and Heliospheric Observatory. The average flow is poleward at all latitudes up to 75°, which suggests that it extends to the poles. It was faster at sunspot cycle minimum than at maximum and substantially faster on the approach to the current minimum than it was at the last solar minimum. This result may help to explain why this solar activity minimum is so peculiar.

The Sun's meridional flow has been difficult to measure (*1*). Its amplitude (10 to 20 m s^{-1}) is more than an order of magnitude weaker than that of the other major flows on the surface of the Sun (granulation ~3000 m s^{-1}, supergranulation ~300 m s^{-1}, and differential rotation ~170 m s^{-1}). In the past, this has led to reports of vastly different flow speeds and directions (*2*–*5*). Despite its weakness, the meridional flow plays a key role in the magnetic evolution of the Sun's surface. It transports magnetic elements that, when carried to the poles, reverse the magnetic polarity of the poles and build up polar fields of opposite polarity after each sunspot cycle maximum. Models of this magnetic flux transport process (*6*–*8*) have employed a variety of substantially different flow profiles. The fidelity of these flux transport models is important because they are used in climate change studies (*9*, *10*) to estimate the total irradiance of the Sun over the past century. The meridional flow is also key to flux transport dynamo models that have been used to predict the amplitude of Solar Cycle 24 (*11*, *12*). An obvious conflict between the surface flux transport models (*6*–*10*) and the flux transport dynamo models (*11*, *12*) is found in their sensitivity to the strength of the meridional flow. A stronger meridional flow produces weaker polar fields in the surface flux transport models, whereas the same flow produces stronger polar fields (and shorter sunspot cycles) in the flux transport dynamos. Solar Cycle 23 (1996 to 2008) provides an interesting problem for all of these models. The strength of the polar fields produced after cycle maximum in 2000–2001 was only about half that seen in the previous three solar cycles (*13*). Furthermore, cycle 24 started much later than average. The late start for cycle 24 has left behind a long quiet minimum unlike any in the past 100 years.

We measured the Sun's meridional flow to determine its variability over Solar Cycle 23 by following the motions of the small magnetic elements that populate the entire surface of the Sun. These are precisely the elements whose motions are modeled in both the surface flux transport models and the flux transport dynamo models. Motions of sunspots, and even the plasma at the surface, are known to differ from those of the small magnetic elements (*1*–*5*). The data we used have been acquired by the Michelson Doppler Imager (MDI) on the European Space Agency (ESA)/National Aeronautics and Space Administration (NASA) Solar and Heliospheric Observatory (SOHO). MDI produces images of the line-of-sight magnetic field across the visible solar disc every 96 min. This is done by measuring differences in circular polarization on either side of a spectral absorption line caused by traces of nickel in the Sun's atmosphere (*14*). We measured the displacement of the magnetic elements by comparing their positions at 8-hour (5-image) intervals from May 1996 to June 2009. The 1024-by-1024 pixel magnetic images were mapped onto a 1024-by-1024 grid in heliographic latitude and longitude from the central meridian. This mapping accounts for changes in the position angle of the Sun's rotation axis relative to the spacecraft's vertical axis, changes in the tilt angle of the Sun's rotation axis toward or away from the spacecraft, and changes in perspective at different distances from the Sun. Because sunspots have very different proper motions (*4*) and produce localized outflows (*15*), we removed sunspots and their immediate surroundings by masking all pixels with measured absolute field strengths greater than 500 Gauss and all contiguous pixels of the same polarity with absolute field strengths above 100 Gauss. Displacements in longitude and

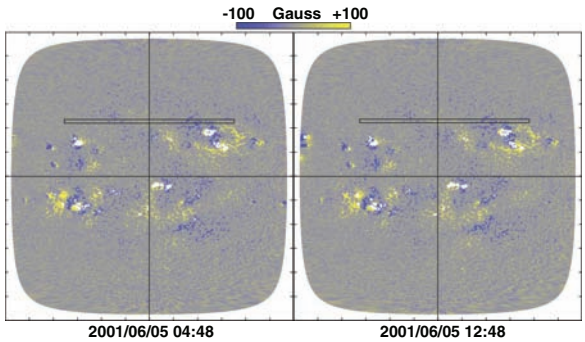

Fig. 1. Magnetic element motion. A pair of masked magnetic maps from 5 June 2001 that were obtained 8 hours apart are shown here with blue representing negative magnetic polarity and yellow representing positive magnetic polarity. The tick marks around the borders are at 15° intervals in latitude and in longitude from the central meridian. The masked-out sunspot areas are evident as white patches. The strongest correlation for the outlined strip of pixels in the earlier map (**left**) is calculated to occur for a shift of 23.7 pixels in longitude and 0.4 pixels in latitude for a similar strip in the later map (**right**).

[1]NASA Marshall Space Flight Center, Huntsville, AL 35812, USA. [2]University of Memphis, Memphis, TN 38152, USA.

*To whom correspondence should be addressed. E-mail: david.hathaway@nasa.gov

Downloaded from www.sciencemag.org on March 12, 2010

latitude were determined for strips (11 pixels high in latitude and 600 pixels long in longitude) by finding the maximum in the cross-correlation with similar strips from the magnetic image acquired 8 hours later (Fig. 1). These calculations were done at 860 latitude positions between ±75° for more than 60,000 image pairs. The meridional flow velocities from these measurements were averaged over individual 27-day rotations of the Sun to extract the axisymmetric signals for each of 167 rotations in the time interval.

The MDI instrument has several known imaging problems (*16*). Our own measurements were most sensitive to the misalignment of the instrument with respect to the star trackers. A small misalignment rotates the 2000 m s^{-1} solar rotation signal into an apparent meridional flow from one hemisphere to the other. Although north-south asymmetries in solar activity do frequently occur, they are usually highly variable and never persist for very long (*17*). We found that a position angle correction of 0.21° counterclockwise [consistent with previous estimates (*16*)] minimized this signal but left a weak trend (from 0.7 m s^{-1} south-to-north in 1996 to 0.7 m s^{-1} north-to-south in 2009). This correction also revealed a significant annual variation (Fig. 2). We attribute this variation to a 0.08° decrease in the accepted tilt of the Sun's equatorial plane relative to the plane of Earth's orbit. This was indicated in a previous study (*18*) based on data from 1996 to 2001 but has not been adopted by the community.

We have constructed the average meridional flow profile (Fig. 3) from those obtained for the individual solar rotations after removing the cross-equatorial signal caused by the annual variation in the error in the tilt angle of the Sun's equatorial plane. This average profile is slightly asymmetric, with a peak velocity of about 12 m s^{-1} in the south and 10 m s^{-1} in the north. The average meridional flow is still poleward at 75° latitude in each hemisphere. This observed profile differs substantially at some latitudes when compared with profiles used in surface flux transport models (*6–10*). These discrepancies, if they exist, represent a challenge for understanding the meridional flow and its effect on the polar fields. An earlier study of the magnetic element motions (*5*) and measurements with helioseismic methods (*19–21*) had suggested this poleward extension, but all of those measurements were confined to latitudes below 60°. Our measurements show that the meridional flow extends well beyond 75° latitude in each hemisphere.

We fit the individual meridional flow profiles with associated Legendre polynomials (*1*) to extract the flow components. By far, the dominant component is that associated with $P_2^1(\theta) = 2\sin\theta\cos\theta$, where θ is the colatitude measured southward from the north pole. The amplitude of this component (Fig. 4) is well determined for each solar rotation and shows a systematic variation over the solar cycle—fast flow at minimum and slow flow at maximum. The flow speed was 11.5 m s^{-1} at Cycle 23 minimum in 1996–1997. It dropped to 8.5 m s^{-1} at Cycle 23 maximum in 2000–2001 and then increased to 13.0 m s^{-1} in 2004 and has maintained that speed. The slowing of the meridional flow from minimum to maximum seems to be a regular occurrence. This was seen in previous solar cycles (*5*), but with less certainty and poorer time resolution. The variations seen from 1996 to 2009 also indicate a difference between Cycle 23 minimum (1996–1997) and Cycle 24 minimum (2008–2009)—the meridional flow has been substantially faster since 2004 than it was during the Cycle 23 minimum. This is consistent with the observed weaker polar fields (*13*) in the surface flux transport models (*6–10*) but leads to conflicts with the flux transport dynamos (*11*, *12*). This fast meridional flow should produce stronger polar fields and a short cycle in the flux transport dynamo models, whereas the observations indicate weak polar fields and a long solar cycle.

The source of the disagreement between the surface flux transport models (*6–10*) and the flux transport dynamo models (*11*, *12*) can be seen in the latitudinal distribution of magnetic polarities in these models. The dynamo models have fields of one polarity centered on the sunspot latitudes, whereas the surface models have bands of opposite magnetic polarity on either side of the sunspot latitudes, as is observed. A fast meridional flow in the dynamo models carries elements of only one polarity to the poles. This rapidly erodes the old polar fields and produces strong polar fields of the opposite polarity. A fast meridional flow in the surface models inhibits opposite polarities from canceling each other across the equator and carries elements of both polarities to the poles (with a slight excess of elements with the polarity of the poleward side of the sunspot latitudes). This requires a longer time to reverse the old polar fields and builds up weaker polar fields of the opposite polarity. The variations we observe in the strength of the poleward meridional flow help the surface flux transport models explain (*22*, *23*) the production of weaker polar fields (*13*) and this long quiet minimum based on the faster meridional flow found after 2004.

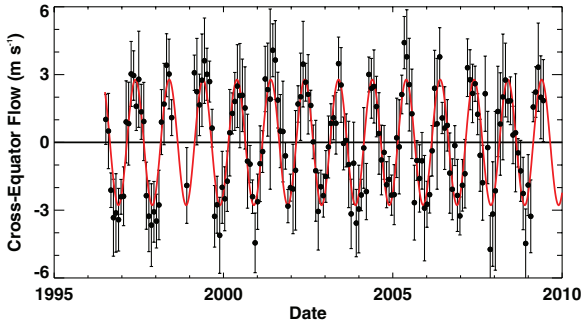

Fig. 2. Annual variation in the cross-equatorial flow. The measured cross-equatorial flow component for each of 167 rotations of the Sun is shown by the filled circles with 2σ error bars. The signal is well fit (red line), with an annual variation produced by a 0.08° decrease in the accepted tilt of the Sun's equatorial plane to the plane of the Earth's orbit. Using the accepted value of 7.25° projects the Sun's rotational velocity into a south-to-north flow in the spring and a north-to-south flow in the fall.

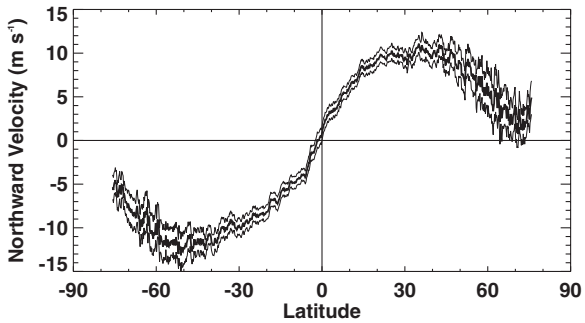

Fig. 3. The average meridional flow profile from 167 rotations of the Sun between May 1996 and June 2009 is shown with the thick line for 860 latitude positions between ±75°. The 2σ error range is indicated by the thin lines.

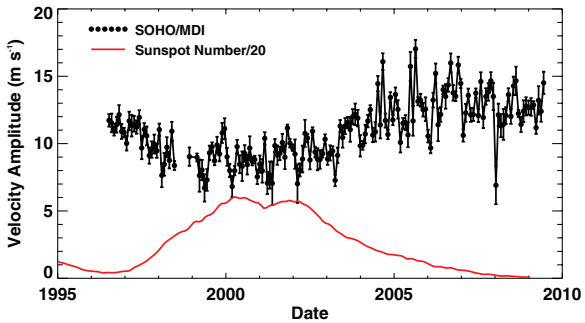

Fig. 4. Meridional flow amplitude variation from May 1996 to June 2009. The amplitude of the primary component of the meridional flow is plotted as dots with 2σ error bars for each solar rotation. The dots are connected except across the SOHO "summer vacation" in 1998. The scaled (by 1/20) smoothed sunspot number is shown in red to indicate the phases of the solar activity cycle.

Downloaded from www.sciencemag.org on March 12, 2010

References and Notes

1. D. H. Hathaway, *Astrophys. J.* **460**, 1027 (1996).
2. K. Topka, R. Moore, B. J. LaBonte, R. Howard, *Sol. Phys.* **79**, 231 (1982).
3. E. Ribes, P. Mein, A. Mangeney, *Nature* **318**, 170 (1985).
4. M. A. Kambry, J. Nishikawa, T. Sakurai, K. Ichimoto, E. Hiei, *Sol. Phys.* **132**, 41 (1991).
5. R. W. Komm, R. F. Howard, J. W. Harvey, *Sol. Phys.* **147**, 207 (1993).
6. C. R. DeVore, N. R. Sheeley Jr., *Sol. Phys.* **108**, 47 (1987).
7. A. A. van Ballegooijen, N. P. Cartledge, E. R. Priest, *Astrophys. J.* **501**, 866 (1998).
8. C. J. Schrijver, A. M. Title, *Astrophys. J.* **551**, 1099 (2001).
9. Y.-M. Wang, J. L. Lean, N. R. Sheeley Jr., *Astrophys. J.* **625**, 522 (2005).
10. J. L. Lean, D. H. Rind, *Geophys. Res. Lett.* **35**, L18701 (2008).
11. M. Dikpati, G. de Toma, P. A. Gilman, *Geophys. Res. Lett.* **33**, L05102 (2006).
12. A. R. Choudhuri, P. Chatterjee, J. Jiang, *Phys. Rev. Lett.* **98**, 131103 (2007).
13. L. Svalgaard, E. W. Cliver, Y. Kamide, *Geophys. Res. Lett.* **32**, L01104 (2005).
14. P. H. Scherrer *et al.*, *Sol. Phys.* **162**, 129 (1995).
15. N. R. Sheeley Jr., *Sol. Phys.* **9**, 347 (1969).
16. MDI Calibration Notes and Known Problems, http://soi.stanford.edu/data/cal
17. D. H. Hathaway, R. M. Wilson, *Sol. Phys.* **224**, 5 (2004).
18. J. G. Beck, P. Giles, *Astrophys. J.* **621**, L153 (2005).
19. P. M. Giles, T. L. Duvall Jr., P. H. Scherrer, R. S. Bogart, *Nature* **390**, 52 (1997).
20. J. Schou, R. S. Bogart, *Astrophys. J.* **504**, L131 (1998).
21. I. González Hernández *et al.*, *Astrophys. J.* **638**, 576 (2006).
22. C. J. Schrijver, Y. Liu, *Sol. Phys.* **252**, 19 (2008).
23. Y.-M. Wang, E. Robbrecht, N. R. Sheeley Jr., *Astrophys. J.* **707**, 1372 (2009).

24. The SOHO/MDI project is supported by NASA grant NAG5-10483 to Stanford University. SOHO is a project of international cooperation between ESA and NASA. L.R. was supported as a summer intern at NASA/Marshall Space Flight Center through the Marshall Space Grant Research Internship Project.

15 September 2009; accepted 13 January 2010
10.1126/science.1181990

Cavity Quantum Electrodynamics with Anderson-Localized Modes

Luca Sapienza,* Henri Thyrrestrup, Søren Stobbe, Pedro David Garcia, Stephan Smolka, Peter Lodahl*

A major challenge in quantum optics and quantum information technology is to enhance the interaction between single photons and single quantum emitters. This requires highly engineered optical cavities that are inherently sensitive to fabrication imperfections. We have demonstrated a fundamentally different approach in which disorder is used as a resource rather than a nuisance. We generated strongly confined Anderson-localized cavity modes by deliberately adding disorder to photonic crystal waveguides. The emission rate of a semiconductor quantum dot embedded in the waveguide was enhanced by a factor of 15 on resonance with the Anderson-localized mode, and 94% of the emitted single photons coupled to the mode. Disordered photonic media thus provide an efficient platform for quantum electrodynamics, offering an approach to inherently disorder-robust quantum information devices.

The interaction between a single photon and a single quantized emitter is the core of cavity quantum electrodynamics (QED) and constitutes a node in a quantum information network (*1*, *2*). So far, cavity QED experiments have been realized with a wide range of two-level systems, including atoms (*3*), ions (*4*), Cooper-pair boxes (*5*), and semiconductor quantum dots (*6*–*8*) coupled to photons confined in a cavity. A common requirement for all these implementations is highly engineered cavities, in some cases requiring nanometer-scale accuracy (*9*). Surprisingly, multiple scattering of photons in disordered dielectric structures offers an alternative route to light confinement. If the scattering is very pronounced, Anderson-localized modes form spontaneously. Anderson localization (*10*) is a multiple-scattering wave phenomenon that has been observed for, e.g., light (*11*), acoustic waves (*12*), and atomic Bose-Einstein condensates (*13*). We have demonstrated cavity QED with Anderson-localized modes by efficiently coupling a single quantum dot (QD) to a disorder-induced cavity mode (*14*) in a photonic crystal waveguide.

DTU Fotonik, Department of Photonics Engineering, Technical University of Denmark, Ørsteds Plads 343, DK-2800 Kgs. Lyngby, Denmark.

*To whom correspondence should be addressed. E-mail: lucs@fotonik.dtu.dk (L.S.); pelo@fotonik.dtu.dk (P.L.)

Photonic crystals are composite nanostructures in which a periodic modulation of the refractive index forms a photonic band gap of frequencies where light propagation is fully suppressed. By deliberately introducing a missing row of holes in a two-dimensional photonic crystal membrane, the periodicity is broken locally and light is guided (Fig. 1A). Such photonic crystal waveguides are strongly dispersive, i.e., light propagation depends sensitively on the optical frequency and can be slowed down. Engineering the photonic crystal waveguide enables the enhancement of light-matter interaction, which is required for high-efficiency single-photon sources (*15*) for quantum information technology (*1*, *16*). In the slow-light regime of photonic crystal waveguides, light propagation is very sensitive to unavoidable structural imperfections (*17*, *18*) and multiple-scattering events randomize propagation (*19*). Although multiple scattering is commonly considered a nuisance for a device, leading to optical losses, here the influence of wave interference in multiple scattering stops light propagation and forms strongly confined Anderson-localized modes (*10*) (Fig. 1B). Anderson-localized modes in a photonic crystal waveguide appear as a result of the primarily one-dimensional nature of the propagation of light provided that the localization length is shorter than the length of the waveguide (*20*).

We deliberately created Anderson-localized modes by fabricating photonic crystal waveguides with a lithographically controlled amount of disorder (Fig. 1B). The hole positions in three rows above and below the waveguide were randomly perturbed with a standard deviation varying between 0 and 6% of the lattice parameter. We investigated the Anderson-localized modes by recording QD photoluminescence spectra under high-excitation power where the feeding from multiple QDs makes Anderson-localized modes appear as sharp spectral resonances (Fig. 1C). The observation of spectrally separated random resonances is a signature of Anderson localization of light (*14*), while the detailed statistics of the intensity fluctuations unambiguously verifies localization even in the presence of absorption (*21*). Figure 1D shows the intensity distribution from spectra recorded at different spatial and spectral positions, which allow us to average over different realizations of disorder. Clear deviations from the Rayleigh distribution predicted for nonlocalized waves are observed. Light is localized if the variance of the normalized intensity fluctuations exceeds the critical value of 7/3 (*21*), and we extract a variance of 5.3, which proves Anderson localization.

Examples of Anderson-localized modes are shown in Fig. 2 as peaks appearing at random spectral positions, although limited to the slow-light regime of the photonic crystal waveguide. The latter property is due to the strongly dispersive behavior of the localization length that is considerably shortened in the slow-light regime. We tuned the spectral range of Anderson-localized modes by controlling the amount of disorder. Even in samples without engineered disorder, intrinsic and thus unavoidable imperfections, such as surface roughness, are sufficient to localize light (*22*).

The important cavity figures-of-merit are the mode volume V and the Q factor. Decreasing V leads to an enhancement of the electromagnetic field and thus improves light-matter coupling. The Q factor is proportional to the cavity storage time of a photon that needs to be increased for cavity QED applications. High Q factors ranging between 3000 and 10,000 are obtained for different degrees of disorder (Fig. 2) and are comparable to state-of-the-art values obtained for traditional photonic crystal nanocavities containing QDs (*7*).

Downloaded from www.sciencemag.org on March 12, 2010